Interaction of Porphine and Its Metal Complexes with C_{60} Fullerene: A DFT Study

Vladimir A. Basiuk*

Instituto de Ciencias Nucleares, Universidad Nacional Autónoma de México, Circuito Exterior C.U., A. Postal 70-543, 04510 México D.F., Mexico

Received: February 3, 2005; In Final Form: March 9, 2005

We performed DFT calculations (BLYP general-gradient approximation in conjunction with a double numerical basis set) for the interaction of free porphine ligand and a number of its metal complexes with C_{60} molecule to analyze how the nature of a central metal ion influences the geometry and electronic characteristics (electrostatic potential and spin density distribution and highest-occupied molecular orbital (HOMO) and lowest-unoccupied molecular orbital (LUMO) structure). We found that the presence of a central metal ion is crucial for a strong interaction. The energy of interaction between H_2P and C_{60} is -0.3 kcal mol^{-1} only, whereas the formation energies for the metal complexes vary from -27.3 kcal mol^{-1} for MnClP·C_{60} to -45.8 kcal mol^{-1} for MnP·C_{60}. As a rule, the formation energy correlates with the separations between porphinate and fullerene molecules; the Mn and Fe complexes exhibit the closest approach of ca. 2.2 Å between the metal ion and carbon atoms of C_{60}. In most porphine−C_{60} complexes studied, the two closest contacts of central metal ion or H are those with carbon atoms of the (6,6) bond; VOP·C_{60} is the only exception, where the closest V···C contacts involve the (5,6) bond. The macrocycle geometry changes, and the magnitude of the effect depends on the central atom, being especially dramatic for Mn, MnCl, and Fe complexes. The shape of LUMOs in most complexes with C_{60} is not affected notably as compared to the LUMO of the isolated C_{60} molecule. In the case of Fe, the HOMO extends from the central atom to two opposite pyrrol rings. At the same time, the HOMO−LUMO gap energy decreases drastically in most cases, by ca. 20−30 kcal mol^{-1}. For electrostatic potential distribution, we systematically observed that the negative lobe contacting C_{60} shrinks, whereas the opposite one becomes notably bigger. In the case of paramagnetic complexes of VO, Mn, FeCl, Co, and Cu, spin density distribution was analyzed as well.

I. Introduction

During the past decade, the interaction of porphyrins and related tetraazamacrocyclic compounds with carbon materials has become a subject for numerous studies, focusing on different physicochemical aspects. An important and extensively explored topic to be mentioned first is the supramolecular assemblies of porphyrins on graphite,[1−7] with an expected impact in such areas as light-emitting diodes, organic displays, thin-film transistors, (photo)catalysts, etc. Another topic deals with molecular complexes of porphyrins with fullerenes,[8−18] targeted to the design of new efficient photosynthetic systems, data storage media, and photovoltaic and electrochemical devices.

Our interest is directed toward the research of new hybrid materials composed of tetraazamacrocyclic compounds, including porphyrins and tubular fullerenes, commonly called carbon nanotubes (CNTs). The tetraazamacrocyclic compounds employed up to now are in most cases transition-metal complexes of phthalocyanines,[19−24] with an emphasis on photoconductivity properties of the CNT−phthalocyanine hybrids.[23,24] A few studies that dealt with porphyrins were reported,[25−27] in which noncovalent porphyrin attachment to functionalized single-walled carbon nanotubes (SWNTs) in solution and the preparation of porphyrin−nanotube nanocomposites,[25] chemical bonding of hemin to CNTs for oxygen detection,[26] and photophysical properties of chemically bonded porphyrins[27] were explored. Recently we studied the interaction of simpler tetraazamacrocyclic compounds with SWNTs.[28,29]

The latter theoretical work[29] was motivated by the need to understand the driving forces of tetraazamacrocycle attachment onto CNT surfaces to develop a rational approach to noncovalent CNT derivatization with these interesting and important compounds. A way to approach this knowledge is to study how the energy of complex formation is influenced by different (aliphatic and aromatic) substituents in the macrocyclic ligand as well by the central metal ion in tetraazamacrocyclic complexes. Therefore, we attempted a systematic theoretical study of interaction of a series of tetraaza[14]annulene ligands (simple analogues of porphyrins and phthalocyanines) and their cobalt(II) complexes with short SWNT models, at the B3LYP/LANL2MB level of theory. By comparison of the calculated adsorption energies, we have found that the adsorption of tetraaza[14]-annulene ligands on SWNTs is insignificantly influenced by the presence of aliphatic (methyl) or/and aromatic (benzo) substituents in the macrocyclic molecules. On the contrary, the adsorption dramatically increases in the case of Co(II) complexes. Substantial changes in their geometry and electronic structure (e.g., an increase in negative electrostatic potential at the exposed macrocycle side) were detected.

One of the next issues to be addressed is the effect of central metal ion on the interaction strength and electronic structure of the complexes. The systematic calculations at a sufficiently high theoretical level, however, are hampered by their high cost. This is especially true for open-shell systems (containing paramagnetic metal ions), which is of special interest in the present

* To whom correspondence may be addressed. Phone: (52) 55 56 22 47 39, ext. 224. Fax: (52) 55 56 16 22 33. E-mail: basiuk@nuclecu.unam.mx.

10.1021/jp050605n CCC: $30.25
Published on Web 04/06/2005

TABLE 1: Formation Energies for Porphine−C_{60} Complexes, Closest Contacts between Central Metal Ion (or H Atom in H_2P) and C_{60} Molecule (M···C_{C60}), as well as *trans*-N−M−N Angles in Porphine−C_{60} Complexes and in Isolated Porphines for Comparison

			N−M−N (deg)	
complex	energy (kcal mol^{-1})	M···C_{C60} (Å)[a]	C_{60} complex	isolated porphine
H_2P·C_{60}	−0.3	3.692, 3.800		
		3.669, 3.785	179.7 (out)[b,c]	178.9, 179.0[b]
MgP·C_{60}	−36.0	3.536, 3.567	179.4, 179.7 (out)	179.7, 180
VOP·C_{60}	−35.8	5.049, 5.435[d]	151.3, 151.5 (out)	151.5
MnP·C_{60}	−45.8	2.180, 2.258	155.5, 162.0 (in)[c]	179.5, 180
MnClP·C_{60}	−27.3	4.169	154.5, 168.9 (out)	162.3, 163.3
FeP·C_{60}	−43.8	2.222	157.5, 165.2 (in)	179.6, 179.9
FeClP·C_{60}	−38.6	4.583	166.5, 166.7 (out)	163.5, 169.4
CoP·C_{60}	−36.8	3.560, 3.880	179.6, 180 (in)	179.7, 180
NiP·C_{60}	−36.0	3.414	179.2, 179.5 (out)	178.8, 178.9
CuP·C_{60}	−34.7	3.301, 3.713	179.5, 179.7 (out)	179.7, 179.9
ZnP·C_{60}	−33.9	3.329	177.4, 178.4 (out)	179.4, 179.6
PdP·C_{60}	−35.6	3.523	179.5, 179.7 (out)	179.8, 180

[a] M is metal ion or H^+. [b] Angles N(1)−H(2)−N(4) and N(1)−H(3)−N(4) in the group of aligned atoms N(1)−H(2)···H(3)−N(4). [c] "Out" denotes the opposite position of metal ion or H^+ to the one of C_{60} molecule, with respect to porphine plane; "in" denotes M or H^+ position between C_{60} and porphine plane. [d] In most porphine−C_{60} complexes studied, two closest contacts of metal or H^+ are those with carbon atoms of the (6,6) bond; VOP·C_{60} is the only exception, where the closest V···C contacts involve the (5,6) bond.

context. This circumstance forces one to look for simplified models. Fullerene C_{60} molecule is a good candidate to model tetraazamacrocycle−SWNT interactions since it matches the most important CNT characteristic feature, namely, its curvature. In addition to that, the presence of five-membered rings makes fullerenes good candidates to study the role of pentagonal defects on CNT interaction with different molecules, a subject widely debated at present.[30−34] Finally, theoretical studies of such systems complement the experimental tetraazamacrocycle−C_{60} chemistry.[8−18]

In the present work, we studied theoretically the interaction of free porphine ligand and a number of its metal complexes with the C_{60} molecule to analyze how the nature of a central metal ion influences the geometry and electronic characteristics (electrostatic potential and spin density distribution, highest-occupied molecular orbital (HOMO) and lowest-unoccupied molecular orbital (LUMO) structure).

II. Computational Details

All the electronic structure calculations were performed using DMol3[35] numerical-based density-functional computer software implemented in the Materials Studio Modeling 3.1 package from Accelrys, Inc. The BLYP general-gradient approximation in conjunction with the double-numerical basis set (all-electron core treatment) was employed. Although the default convergence settings worked well in many cases, we found convergence problems when optimizing the systems containing paramagnetic metal ions V(IV), Mn(II), Fe(III), Co(II), and Cu(II); a way to over-ride them was to increase the maximum number of iterations and self-consistent field cycles to 1000.

Formation energies $\Delta E_{complex}$ for the complexes with C_{60} were calculated according to the following formula

$$\Delta E_{complex} = E_{complex} - (E_{C_{60}} + E_P)$$

where E is the corresponding absolute energy and P is the porphine ligand or its metal derivative.

III. Results and Discussion

Along with free porphine ligand (H_2P), we studied a series of its metal complexes, whose selection was based on the occurrence in porphyrin-based natural systems, commercial availability (reflecting their stability and ease of preparation), and the frequency of mention in scientific literature. Thus, the magnesium(II) (MgP), iron(II) (FeP), iron(III) chloride (FeClP), and copper(II) porphinates (CuP) were selected due to the importance of chlorophyll−, iron−, and copper−porphyrin cytochromes for the living nature. Porphinates of vanadium-(IV) (as vanadyl complex VOP), manganese(II) (MnP), manganese(III) chloride (MnClP), cobalt(II) (CoP), nickel(II) (NiP), zinc(II) (ZnP), and palladium(II) (PdP) are as a whole frequently studied compounds (most usually *meso*-tetraphenylporphinates), with a detailed structural information available not only for the isolated compounds but also for their molecular complexes with fullerenes.[8,10−12,14,17,18] Most compounds studied in the present work are closed-shell systems; the exceptions are VOP, MnP, FeClP, CoP, and CuP containing paramagnetic metal ions (spin multiplicity of 2).

Isolated H_2P and its complexes, which do not contain axial ligands, are known to have planar geometry. This is true for the optimized structures and can be appreciated from Figure 1. The angles N(1)—H(2)—N(4) and N(1)—H(3)—N(4) in the group of aligned atoms N(1)—H(2)···H(3)—N(4) of H_2P as well as *trans*-N—M—N angles for M(II)═Mg, Mn, Fe, Co, Ni, Cu, Zn, and Pd are very close to 180° (Table 1). The exceptions are VOP, MnClP, and FeClP, where *trans*-N—M—N angles vary from 151.1° (VOP) to 169.4° (FeClP). The interaction with C_{60} influences the porphine geometry, but the magnitude of the

TABLE 2: HOMO and LUMO Energies (in Hartrees) and HOMO−LUMO Gap (in Hartrees and kcal mol^{-1}) for Isolated Porphines, C_{60}, and Corresponding Porphine−C_{60} Complexes

	isolated porphine			C_{60} complex		
	HOMO (Ha)	LUMO (Ha)	gap (Ha/kcal mol^{-1})	HOMO (Ha)	LUMO (Ha)	gap (Ha/kcal mol^{-1})
H_2P	−0.1677	−0.0991	0.0686/43.0	−0.1704	−0.1352	0.0352/22.1
MgP	−0.1791	−0.1080	0.0711/44.6	−0.1811	−0.1617	0.0194/12.2
VOP	−0.1691[a]	−0.1172[a]	0.0519/32.6	−0.1696[a]	−0.1654[a]	0.0042/2.6
MnP	−0.1626[b]	−0.1213[a]	0.0413/25.9	−0.1805[b]	−0.1524[a]	0.0281/17.6
MnClP	−0.1773	−0.1387	0.0386/24.2	−0.1642	−0.1638	0.0004/0.3
FeP	−0.1814	−0.1338	0.0476/29.9	−0.1948	−0.1545	0.0403/25.3
FeClP	−0.1784[b]	−0.1520[b]	0.0264/16.6	−0.1838[b]	−0.1648[a]	0.0190/11.9
CoP	−0.1785[b]	−0.1130[b]	0.0655/41.1	−0.1835[b]	−0.1583[b]	0.0252/15.8
NiP	−0.1677	−0.1043	0.0634/39.8	−0.1719	−0.1547	0.0172/10.8
CuP	−0.1675[a]	−0.1246[b]	0.0429/26.9	−0.1707[a]	−0.1556[a]	0.0151/9.5
ZnP	−0.1798	−0.1058	0.0740/46.4	−0.1822	−0.1543	0.0279/17.5
PdP	−0.1840	−0.1067	0.0773/48.5	−0.1875	−0.1554	0.0321/20.1
C_{60}				−0.2068	−0.1419	0.0649/40.7

[a] α-spin orbitals. [b] β-spin orbitals.

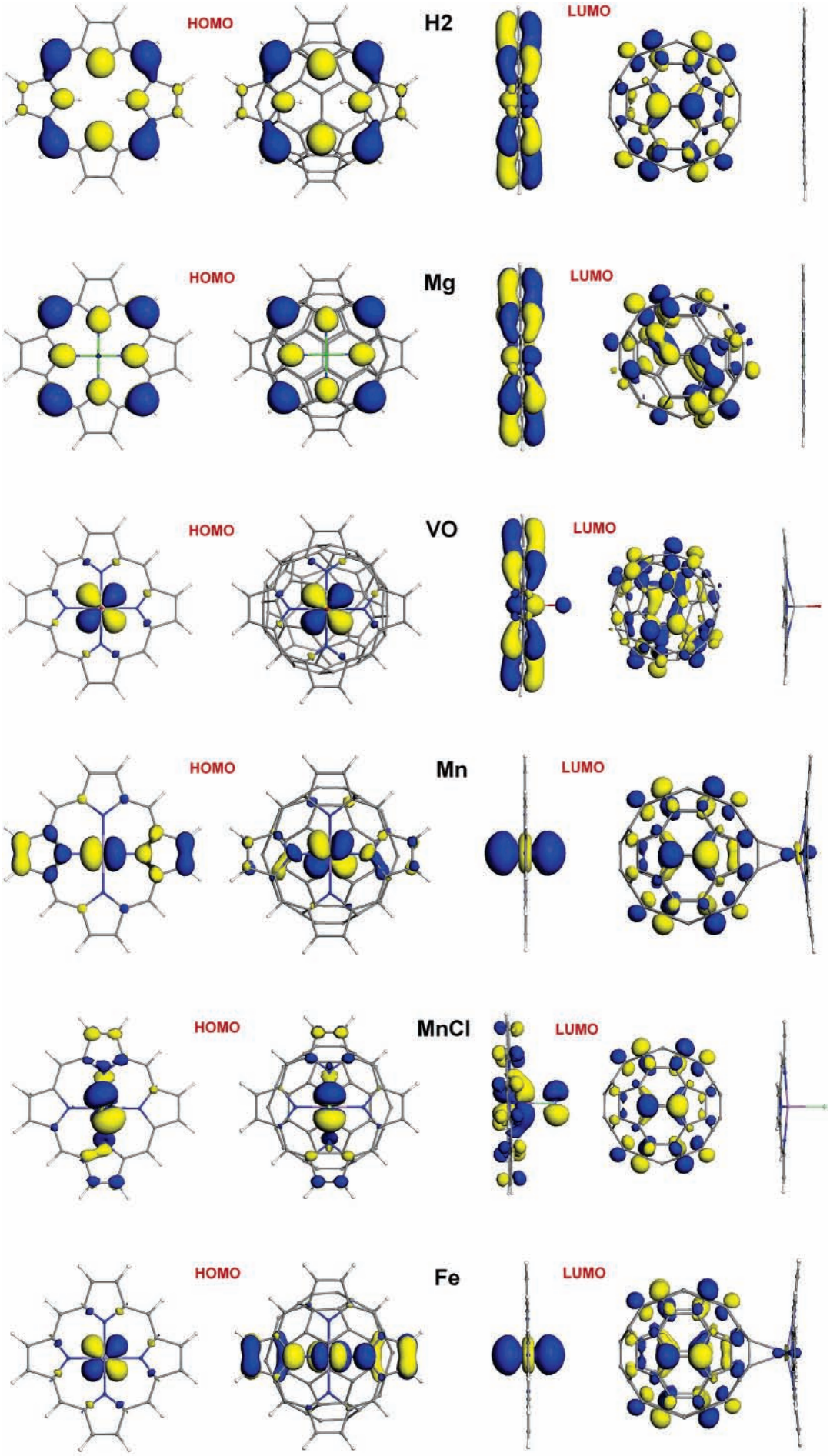
HOMO
H2
LUMO
HOMO
Mg
LUMO
HOMO
VO
LUMO
HOMO
Mn
LUMO
HOMO
MnCl
LUMO
HOMO
Fe
LUMO

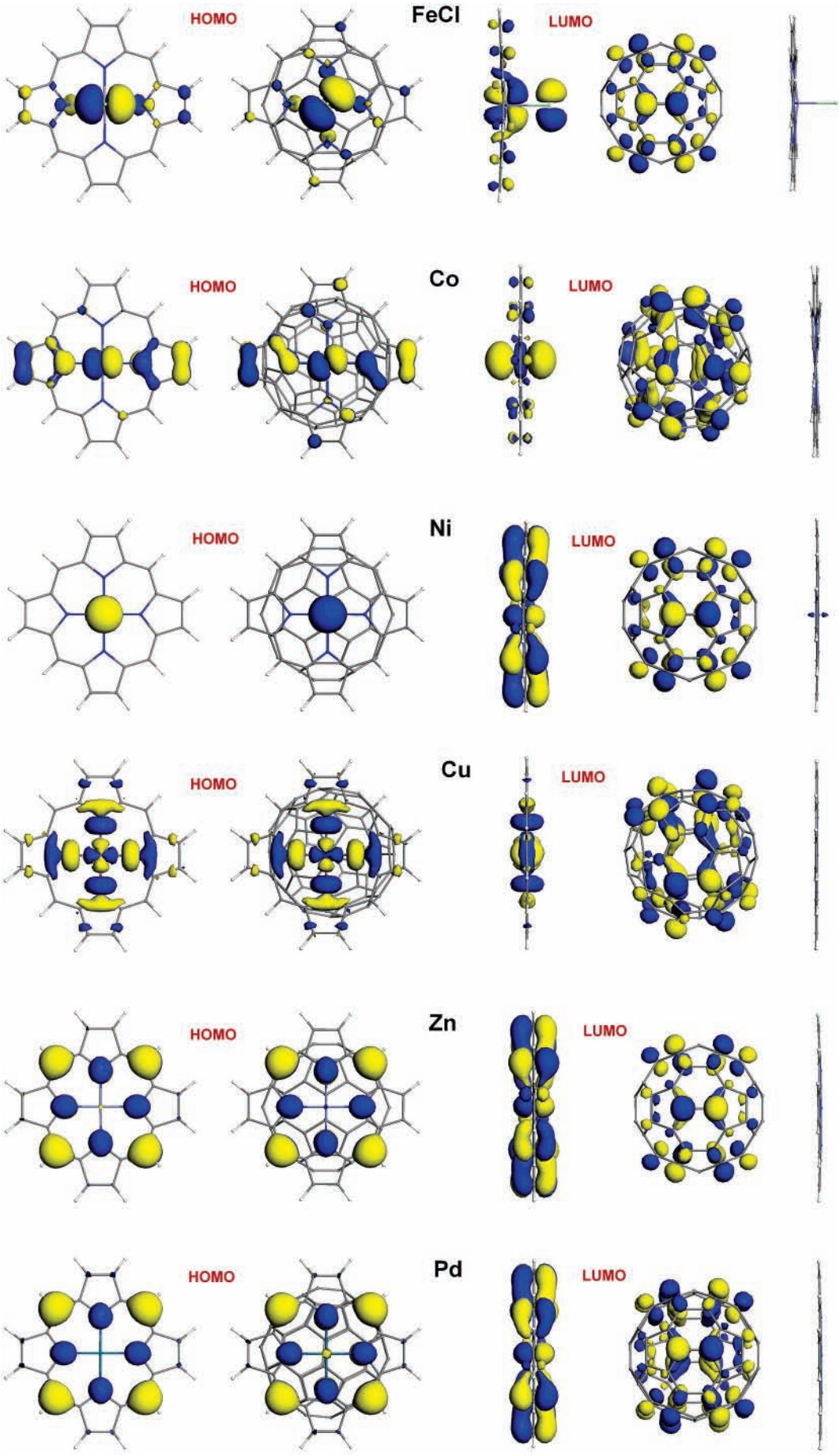

Figure 1 Continued. General views of the optimized geometries and HOMO−LUMO structure (isosurfaces at 0.03 au) for isolated porphine molecules and their complexes with C_{60}.

effect depends on the central atom. In terms of N—H—N and N—M—N angles, only insignificant (less than 0.5°) changes can be observed for H_2P and its complexes with Mg, VO, Co, Ni, Cu, and Pd (Table 1). Interestingly, even though for CoP·C_{60} the angle changes are negligible, one can notice a strong saddlelike distortion of the porphine ring (Figure 1). A moderate N—M—N decrease by 1−3° was found for FeCl (the saddlelike distortion is evident) and Zn complexes. Finally, it becomes dramatic for Mn, MnCl, and Fe complexes, with the strongest N—M—N decrease by almost 25° for the M(II) complexes (Table 1). Along with the latter phenomenon, the Mn and Fe complexes exhibit the closest approach of ca. 2.2 Å between the metal ion and carbon atoms of C_{60}. (In most porphine−C_{60} complexes studied here, the two closest contacts of central metal ion or H are those with carbon atoms of the (6,6) bond; VOP·C_{60} is the only exception, where the closest V···C contacts involve the (5,6) bond.) On the other hand, this strong interaction pulls Mn and Fe atoms out from the macrocyclic plane, as any common monodentate ligand does (e.g., O and Cl in VOP, MnClP, and FeClP). Besides these two cases, the central ion was found between C_{60} and porphine plane for CoP only; in all other cases (including H_2P) it occupies the opposite position (Table 1).

The closest M···C_{C60} distances vary rather widely, from ca. 2.2 Å for the Mn and Fe complexes to more than 5 Å for VOP·C_{60}. The values higher than 4 Å were found for MnClP·C_{60} and FeClP·C_{60}; in other words, the presence of O and Cl as axial ligand weakens the interaction between porphinate and fullerene. For the remaining complexes, M···C_{C60} separations are observed in the range of 3.3−3.9 Å. Unfortunately, X-ray structural data for the H_2P·C_{60} molecular complex and its metal derivatives are unavailable, so we can only compare the calculated M···C_{C60} distances from Table 1 with the reported experimental values for other porphyrin−fullerene complexes (mainly derivatives of *meso*-tetraarylporphines and octaalkylporphyrins). The latter values typically range from 2.6 to 3.3 Å in the absence of axial ligands,[8,10,12,17,18] slightly increasing to 2.8−3.5 Å for Zn and Fe complexes containing axial ligands such as pyridine, O, etc.[8,10,14] The difference between the experimental and calculated values is evidently due to a dense packing of porphyrin and fullerene molecules in the crystalline phase, facilitated by additional van der Waals interactions between fullerenes and aromatic/aliphatic substituents of the porphyrins.

As it was expected (and is consistent with our earlier theoretical results for the interaction of simpler teraazamacrocyclic compounds with SWNTs[29]), in thermodynamic terms, the interaction of H_2P with C_{60} is extremely weak (the energy of complex formation of −0.3 kcal mol^{-1}, Table 1) contrary to all the metal complexes. The formation energies for the latter vary from −27.3 kcal mol^{-1} (MnClP·C_{60}) to −45.8 kcal mol^{-1} (MnP·C_{60}). We analyzed a graphic inter-relation between the energy of porphinate−C_{60} complex formation and the closest contacts between central metal ion and C_{60} molecule (Figure 2) and found that higher formation energies are as a rule associated with shorter M···C_{C60} distances. From the plot, one can also see that in the case of open-shell system the interaction is generally stronger than for the closed-shell ones (compare Mn vs Fe, FeCl vs MnCl, Co vs Ni, and Cu vs Zn, respectively). The points for VO and FeCl do not fit into the trend.

The shape of the frontier HOMO and LUMO can be used to test for the existence of interactions between porphyrin system and C_{60}, as suggested by D'Souza et al.[36] for covalently linked porphyrin−C_{60} dyads. From Figure 1, one can see different

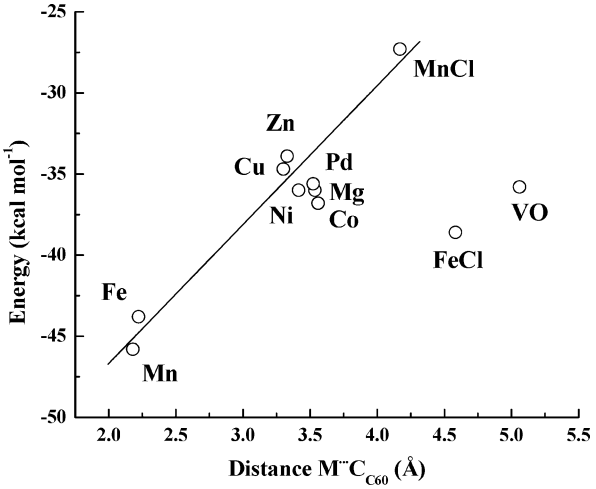

Figure 2. Graphic inter-relation between the energy of porphinate−C_{60} complex formation and the closest contacts between central metal ion and C_{60} molecule. In cases when the metal ion approaches two C_{60} atoms at different M···C_{C60} distances (Table 1; for Mg, VO, Mn, Co, and Cu), the shortest distances were used for the plot.

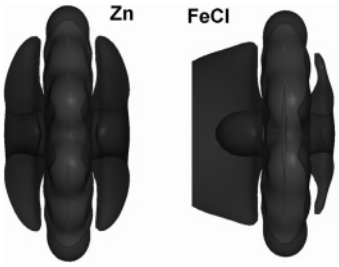

Figure 3. Molecular electrostatic potential isosurfaces (at 0.015 au) for isolated molecules of two representative porphinates, ZnP and FeClP. Side lobes correspond to negative potential, whereas positive potential is associated with the porphine plane.

patterns of HOMO and LUMO behavior as a function of the central atom. The porphine system is more reactive with respect to electrophilic reagents, whereas the C_{60} molecule is more reactive toward nucleophilic reagents. Correspondingly, HOMOs of porphinate−C_{60} complexes remain at the teraazamacrocyclic component, whereas LUMOs can be found almost exclusively at C_{60}. However in two cases of Mn and Fe, we detected a notable LUMO transfer to the metal atom. Thus one can expect that coordination of an additional axial ligand or nucleophilic attack on the Mn and Fe atoms here is facilitated as compared to other porphinate−C_{60} complexes studied. The shape of LUMOs in most complexes with C_{60} does not undergo any substantial changes as compared to the LUMO of the isolated C_{60} molecule (with the exception of the Mg complex, which is the only s element among the metals considered). With regard to HOMOs, the most evident change can be seen for Fe, where the HOMO extends from the central atom to two opposite pyrrol rings. In the case of the Mn, MnCl, FeCl, and Co complexes, moderate changes are mainly due to rotation of the central lobes. In the remaining porphinate−C_{60} complexes and H_2P·C_{60}, the HOMO shape keeps the features typical for isolated porphine molecules.

In numerical terms, that is HOMO−LUMO gap energies, much more drastic changes can be found in most cases (Table 2). Although the gap energy decrease caused by the interaction with C_{60} varies very widely, from 4.6 kcal mol^{-1} for the Fe complex to 32.4 kcal mol^{-1} for the Mg complex, in most cases it lies between 20 and 30 kcal mol^{-1}. Both iron complexes differ from others by the smallest gap energy decrease of 4.6−

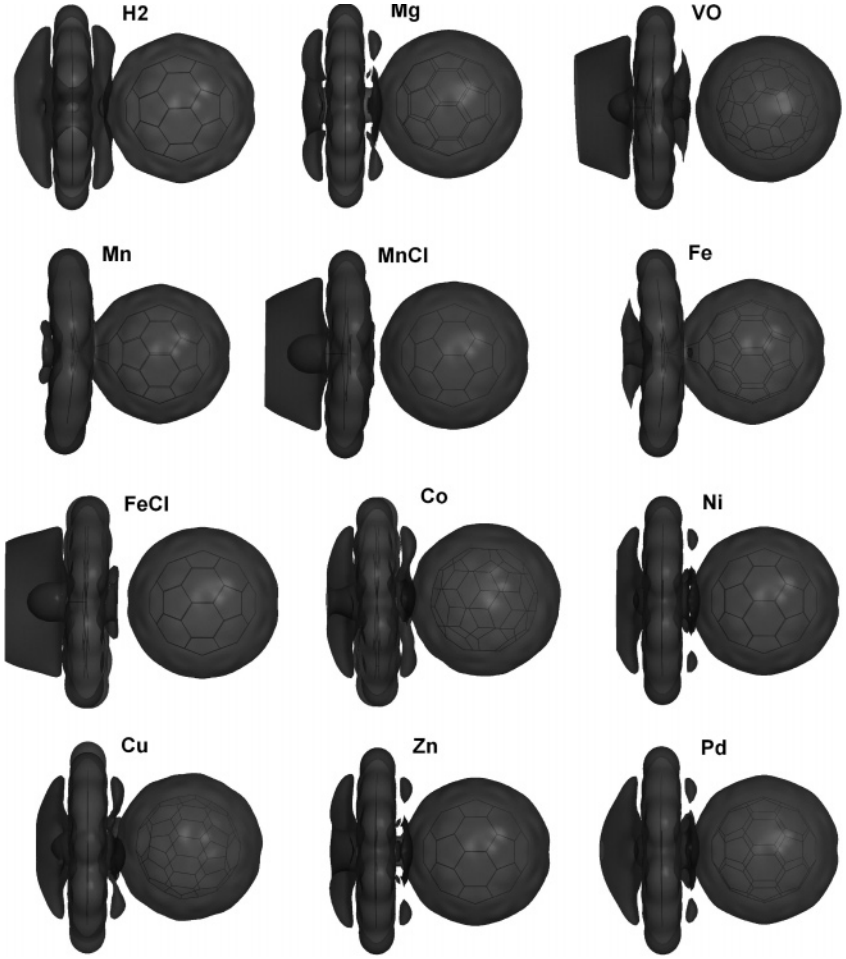

Figure 4. Molecular electrostatic potential isosurfaces (at 0.015 au) for the complexes of H_2P and metal porphinates with C_{60} molecule. Side lobes in the porphines correspond to negative potential, whereas positive potential is associated with the porphine plane and C_{60} molecule.

4.7 kcal mol^{-1}. The manganese complexes behave less uniformly, where it is 8.3 kcal mol^{-1} for the Mn complex and 23.9 kcal mol^{-1} for the MnCl complex. The final gap energy is the smallest in the latter case, of 0.3 kcal mol^{-1} only, whereas in such cases as $H_2P{\cdot}C_{60}$ and the complexes of Mg, Mn, Fe, FeCl, Co, Ni, Zn, and Pd the gap energy remains higher than 10 kcal mol^{-1}.

The next manifestation of the interactions between porphine and fullerene systems can be visualized by plotting molecular electrostatic potential. The isosurfaces (at 0.015 au) for isolated molecules of two representative porphinates are shown in Figure 3. Negative potential (side lobes) is always associated with the coordination sphere, that is, with the nitrogen donor atoms and metal ion. For H_2P, as well as for Mg, Mn, Fe, Co, Ni, Cu, Zn, and Pd porphinates, negative electrostatic potential is distributed symmetrically with respect to the macrocyclic plane. In three cases of VO, MnCl, and FeCl, the negative lobes are asymmetric, with the bigger one comprising the highly electronegative O and Cl atoms. The interaction with the fullerene molecule results in a strong shrinking of the negative lobe contacting C_{60}, whereas the opposite one becomes notably bigger (Figure 4). A similar phenomenon was observed for Co(II) complexes of tetraaza[14]annulenes adsorbed on SWNTs.[29]

Five of the porphinates studied contain paramagnetic metal ions, namely, VOP, MnP, FeClP, CoP, and CuP. We calculated spin density distribution before and after complexation with C_{60}. In Figure 5, the corresponding isosurface plots at 0.002 au are shown. In CoP, the spin density is concentrated on the Co atom, without notable extension to other parts of the molecule. $CoP{\cdot}C_{60}$ keeps this feature, but in addition to that, an increased positive spin density can be detected at neighboring atoms of C_{60}. This effect is much more visible in the case of Mn; the complexation with C_{60} also gives rise to a dramatic redistribution of spin density within the MnP component, by its transfer to two opposite pyrrol rings. A more moderate redistribution was found for FeCl, whereas for the VO and Cu complexes, no changes were observed at all. (One should note that the spin density distribution in CuP differs considerably from that in other paramagnetic porphinates analyzed: it exhibits a relatively low spin density at the central atom, and at the same time, a very high spin density at all four nitrogen donor atoms. It this sense, CuP behaves as the antipode of CoP.)

IV. Conclusions

According to our DFT calculations of the interaction of free porphine ligand and a number of its metal complexes with the C_{60} molecule, the presence of a central metal ion is crucial for the attraction to be strong. While the energy of interaction between H_2P and C_{60} is -0.3 kcal mol^{-1} only, the formation energies for the metal complexes vary from -27.3 kcal mol^{-1} ($MnClP{\cdot}C_{60}$) to -45.8 kcal mol^{-1} ($MnP{\cdot}C_{60}$). As a rule, these values correlate with the separations between porphinate and fullerene molecules; the Mn and Fe complexes exhibit the closest approach of ca. 2.2 Å between the metal ion and carbon atoms of C_{60}. The porphine geometry changes, and the magnitude of the effect depends on the central atom, being especially dramatic for Mn, MnCl, and Fe complexes.

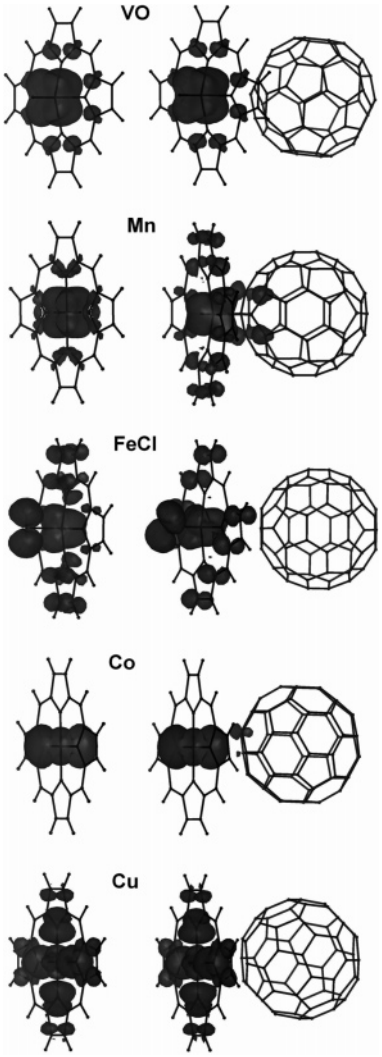

Figure 5. Spin-density distribution (isosurface at 0.002 au) in VOP, MnP, FeClP, CoP, and CuP before (left plots) and after complexation with C_{60} (right plots).

Considerable changes are observed in the electronic structure of the complexes. The HOMO and LUMO shape, gap energy, electrostatic potential, and spin-density distribution were analyzed. The shape of LUMOs in most complexes with C_{60} does not undergo any substantial changes as compared to the LUMO of the isolated C_{60} molecule. In the case of Fe, the HOMO extends from the central atom to two opposite pyrrol rings. At the same time, the HOMO−LUMO gap energy decreases drastically in most cases, by ca. 20−30 kcal mol^{-1}. For electrostatic potential distribution, we systematically observed that the negative lobe contacting C_{60} shrinks, whereas the opposite one becomes notably bigger. In the case of paramagnetic complexes of VOP, MnP, FeClP, CoP, and CuP, some changes were detected in the spin density distribution.

Acknowledgment. Financial support from the National Council of Science and Technology of Mexico (Grants CONACYT-36317-E and -40399-Y) and from the National Autonomous University of Mexico (Grants DGAPA-IN100402-3 and -IN100303) is greatly appreciated.

References and Notes

(1) Lei, S. B.; Wang, C.; Yin, S. X.; Wang, H. N.; Xi, F.; Liu, H. W.; Xu, B.; Wan, L. J.; Bai, C. L. *J. Phys. Chem. B* **2001**, *105*, 10838.

(2) Wang, H.; Wang, C.; Zeng, Q.; Xu, S.; Yin, S.; Xu, B.; Bai, C. *Surf. Interface Anal.* **2001**, *32*, 266.

(3) Lei, S. B.; Wang, J.; Dong, Y. H.; Wang, C.; Wan, L. J.; Bai, C. L. *Surf. Interface Anal.* **2002**, *34*, 767.

(4) Elemans, J. A. A. W.; Lensen, M. C.; Gerritsen, J. W.; van Kempen, H.; Speller, S.; Nolte, R. J. M.; Rowan, A. E. *Adv. Mater.* **2003**, *15*, 2070.

(5) Guo, Q.; Yin, J.; Yin, F.; Palmer, R. E.; Bampos, N.; Sanders, J. K. M. *J. Phys.: Condens. Matter* **2003**, *15*, S3127.

(6) Yin, J.; Guo, Q.; Palmer, R. E.; Bampos, N.; Sanders, J. K. M. *J. Phys. Chem. B* **2003**, *107*, 209.

(7) Ikeda, T.; Asakawa, M.; Goto, M.; Miyake, K.; Ishida, T.; Shimizu, T. *Langmuir* **2004**, *20*, 5454.

(8) Konarev, D. V.; Yudanova, E. I.; Neretin, I. S.; Slovokhotov, Yu. L.; Lyubovskaya, R. N. *Synth. Met.* **2001**, *121*, 1125.

(9) Kubo, Y.; Sugasaki, A.; Ikeda, M.; Sugiyasu, K.; Sonoda, K.; Ikeda, A.; Takeuchi, M.; Shinkai, S. *Org. Lett.* **2002**, *4*, 925.

(10) Konarev, D. V.; Kovalevsky, A. Yu.; Li, X.; Neretin, I. S.; Litvinov, A. L.; Drichko, N. V.; Slovokhotov, Yu. L.; Coppens, P.; Lyubovskaya, R. N. *Inorg. Chem.* **2002**, *41*, 3638.

(11) Sun, D.; Tham, F. S.; Reed, C. A.; Boyd, P. D. W. *Proc. Natl. Acad. Sci. U.S.A.* **2002**, *99*, 5088.

(12) Ishii, T.; Aizawa, N.; Kanehama, R.; Yamashita, M.; Sugiura, K.-i.; Miyasaka, H. *Coord. Chem. Rev.* **2002**, *226*, 113.

(13) Hasobe, T.; Imahori, H.; Fukuzumi, S.; Kamat, P. V. *J. Phys. Chem. B* **2003**, *107*, 12105.

(14) Lee, H. M.; Olmstead, M. M.; Gross, G. G.; Balch, A. L. *Cryst. Growth Des.* **2003**, *3*, 691.

(15) Hasobe, T.; Kamat, P. V.; Absalom, M. A.; Kashiwagi, Y.; Sly, J.; Crossley, M. J.; Hosomizu, K.; Imahori, H.; Fukuzumi, S. *J. Phys. Chem. B* **2004**, *108*, 12865.

(16) Yoshimoto, S.; Saito, A.; Tsutsumi, E.; D'Souza, F.; Ito, O.; Itaya, K. *Langmuir* **2004**, *20*, 11046.

(17) Konarev, D. V.; Litvinov, A. L.; Neretin, I. S.; Drichko, N. V.; Slovokhotov, Yu. L.; Lyubovskaya, R. N.; Howard, J. A. K.; Yufit, D. S. *Cryst. Growth Des.* **2004**, *4*, 643.

(18) Neretin, I. S.; Slovokhotov, Yu. L. *Russ. Chem. Rev.* **2004**, *73*, 455.

(19) Wang, X.; Liu, Y.; Qiu, W.; Zhu, D. *J. Mater. Chem.* **2002**, *12*, 1636.

(20) Cao, L.; Chen, H.-Z.; Zhou, H.-B.; Zhu, L.; Sun, J.-Z.; Zhang, X.-B.; Xu, J.-M.; Wang, M. *Adv. Mater.* **2003**, *15*, 606.

(21) Cao, L.; Chen, H.-Z.; Li, H.-Y.; Zhou, H.-B.; Sun, J.-Z.; Zhang, X.-B.; Wang, M. *Chem. Mater.* **2003**, *15*, 3247.

(22) De la Torre, G.; Blau, W.; Torres, T. *Nanotechnology* **2003**, *14*, 765.

(23) Cao, L.; Chen, H.; Wang, M.; Sun, J.; Zhang, X.; Kong, F. *J. Phys. Chem. B* **2002**, *106*, 8971.

(24) Yang, Z.-L.; Chen, H.-Z.; Cao, L.; Li, H.-Y.; Wang, M. *Mater. Sci. Eng. B* **2004**, *106*, 73.

(25) Murakami, H.; Nomura, T.; Nakashima, N. *Chem. Phys. Lett.* **2003**, *378*, 481.

(26) Ye, J.-S.; Wen, Y.; Zhang, W. D.; Cui, H.-F.; Gan, L. M.; Xu, G. Q.; Sheu, F.-S. *J. Electroanal. Chem.* **2004**, *562*, 241.

(27) Li, H.; Martin, R. B.; Harruff, B. A.; Carino, R. A.; Allard, L. F.; Sun Y.-P. *Adv. Mater.* **2004**, *16*, 896.

(28) Basiuk, E. V.; Rybak-Akimova, E. V.; Basiuk, V. A.; Acosta-Najarro, D.; Saniger, J. M. *Nano Lett.* **2002**, *2*, 1249.

(29) Basiuk, V. A. *J. Phys. Chem. B* **2004**, *108*, 19990.

(30) Grujicic, M.; Cao, G.; Rao, A. M.; Tritt, T. M.; Nayak, S. *Appl. Surf. Sci.* **2003**, *214*, 289.

(31) Lu, X.; Chen, Z.; Schleyer, P. v. R. *J. Am. Chem. Soc.* **2005**, *127*, 20.

(32) Picozzi, S.; Santucci, S.; Lozzi, L.; Valentini, L.; Delley, B. *J. Chem. Phys.* **2004**, *120*, 7147.

(33) Basiuk, E. V.; Monroy-Peláez, M.; Puente-Lee, I.; Basiuk, V. A. *Nano Lett.* **2004**, *4*, 863.

(34) Basiuk, E. V.; Gromovoy, T. Yu.; Datsyuk, A.; Palyanytsya, B. B.; Pokrovskiy, V. A.; Basiuk, V. A. *J. Nanosci. Nanotechnol.* **2005**, accepted.

(35) (a) Delley, B. *J. Chem. Phys.* **1990**, *92*, 508. (b) http://www.accelrys.com/mstudio/ms_modeling/dmol3.html.

(36) D'Souza, F.; Gadde, S.; Zandler, M. E.; Klykov, A.; El-Khouly, M. E.; Fujitsuka, M.; Ito, O. *J. Phys. Chem. A* **2002**, *106*, 12393.